

Influence of substrate potential shape on the dynamics of a sliding lubricant chain

Rosalie Laure Woulaché,^{1,2} Andrea Vanossi,^{3,4} and Nicola Manini^{3,4,5}

¹ *Laboratoire de Mécanique, Département de Physique, Faculté des Sciences,
Université de Yaoundé I. B.P. 812, Yaoundé, Cameroun*

² *The Abdus Salam International Centre for Theoretical Physics, Strada Costiera, 11-34014 Trieste, Italy**

³ *CNR-IOM Democritos National Simulation Center, Via Bonomea 265, 34136 Trieste, Italy*

⁴ *International School for Advanced Studies (SISSA), Via Bonomea 265, 34136 Trieste, Italy*

⁵ *Dipartimento di Fisica, Università degli Studi di Milano, Via Celoria 16, 20133 Milano, Italy*

(Dated: May 18, 2018)

We investigate the frictional sliding of an incommensurate chain of interacting particles confined in between two nonlinear on-site substrate potential profiles in relative motion. We focus here on the class of Remoissenet-Peyrard parametrized potentials $V_{RP}(x, s)$, whose shape can be varied continuously as a function of s , recovering the sine-Gordon potential as particular case. The observed frictional dynamics of the system, crucially dependent on the mutual ratios of the three periodicities in the sandwich geometry, turns out to be significantly influenced also by the shape of the substrate potential. Specifically, variations of the shape parameter s affects significantly and not trivially the existence and robustness of the recently reported velocity quantization phenomena [Vanossi *et al.*, Phys. Rev. Lett. **97**, 056101 (2006)], where the chain center-of-mass velocity to the externally imposed relative velocity of the sliders stays pinned to exact “plateau” values for wide ranges of the dynamical parameters.

PACS numbers: 68.35.Af, 05.45.-a, 62.20.Qp, 62.25.-g

I. INTRODUCTION

Sliding friction has been a broadly-studied field due to its huge practical relevance as well as its theoretical challenges [1, 2]. The regime of validity and the microscopic origin of the Amontons-Coulomb empirical laws of static and dynamic friction have still open issues [3, 4]. The advancements of technology in the last few decades has triggered both theoretical [5–11] as well as experimental [12–14] investigations in this field.

A broad range of investigations focuses on a simple fundamental model for microscopic tribological system: the Frenkel-Kontorova (FK) model [15] and its extensions [16]. Its standard 1D version consists of a chain of harmonically interacting atoms subject to one periodic sinusoidal potential, thereby representing a discretized elastic overlayer deposited on a corrugated surface. The application of a constant force to the chain allows us to determine a depinning threshold, representative of static friction. For an irrational ratio between the natural atomic spacing and the period of the substrate potential (incommensurate interface), the FK model undergoes a phase transition, called Aubry transition, where the ground state “hull function” exhibits analyticity breaking [17]. When, for a fixed interparticle chain stiffness, the amplitude of the sinusoidal potential is smaller than a certain critical value, the static frictional force vanishes, leading to the onset of free sliding or “superlubricity”; otherwise the chain is pinned until a finite threshold force is overcome.

Superlubricity connected with incommensurability is one of the pervasive concepts of modern tribology with a wide area of relevant practical applications as well as fundamental theoretical issues [18]. The role of incommensurability has been recently extended [19] in the framework of a driven 1D confined model inspired by the tribological problem of two sliding interfaces with a thin lubricant layer in between. The moving interface is thus characterized by three inherent length scales: the periods of the bottom and top substrates, and the period of the embedded solid lubricant structure. In particular, in the presence of a uniform external driving of the top substrate, the interplay between these incommensurate length scales can give rise to intriguing dynamical phase-locking phenomena and surprising velocity “quantization” effects, due to the dragging of topological solitons (“kinks” and “antikinks”), i.e., nonlinear localized density superstructures arising from geometrical lattice mismatch [20–25].

These results are suggestive but remain rather idealized in several respects. In particular, the profile of the corrugation potential energy experienced by a lubricant atom interacting with real physical surfaces is likely to deviate considerably from the sinusoids of the two-substrate confined tribological model. It is therefore useful to investigate what influence the shape of the substrate corrugation may have on the frictional dynamics. In this paper we model the corrugation of the two confining substrates via the Remoissenet-Peyrard (RP) function [26, 27], whose shape can be varied continuously as a function of a parameter. The RP potential, which retrieves the sine-Gordon shape as a special case, has been employed widely and successfully to model the dynamics of atoms adsorbed on crystal surfaces in realistic situa-

*Electronic address: rwoulach@yahoo.com; rwoulach@ictp.it

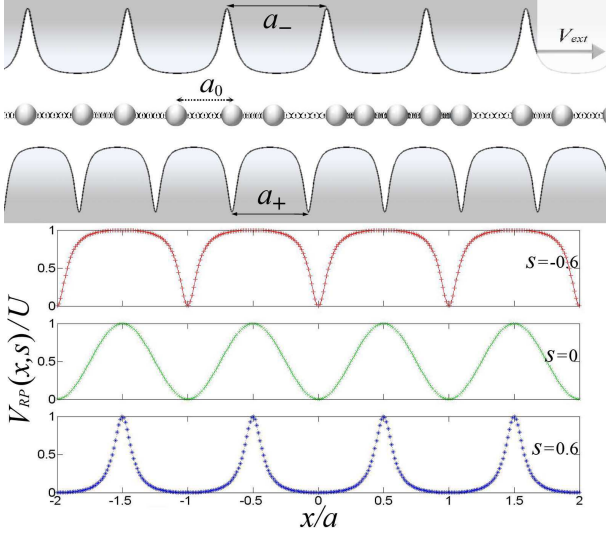


FIG. 1: (Color online) Scheme of the model with three characteristic length scales a_+ (spatial period of the static substrate), a_0 (the equilibrium spacing of the harmonic chain representing the lubricant film), and a_- (spatial period of the advancing substrate). The substrate corrugation is modeled by the RP potential, which is illustrated below for three values of the deformation parameter. Top to bottom $s = -0.6$ (narrow valleys), 0 (pure sine), and 0.6 (broad valleys).

tions [16, 28–30].

II. THE MODEL

Consider the one-dimensional generalization of the two-sines FK model, as in Ref. [20], consisting here of two RP substrate potentials, of spatial periodicity a_+ and a_- and a chain of interacting particles of mass m and harmonic spring constant K , equally spaced by a lattice constant a_0 , mimicking the sandwiched lubricant layer as shown in Fig. 1. The motion of the i -th lubricant particle is governed by

$$m\ddot{x}_i = -\frac{dV_{\text{RP}+}(x_i - v_+t, s)}{dx} - \frac{dV_{\text{RP}-}(x_i - v_-t, s)}{dx} + K(x_{i+1} + x_{i-1} - 2x_i) - \gamma(2\dot{x}_i - v_+ - v_-). \quad (1)$$

Here the RP potential [26] $V_{\text{RP}}(x, s)$ is defined by

$$V_{\text{RP}\pm}(x, s) = \frac{U}{2} \frac{(1-s)^2 [1 - \cos(k_{\pm}x)]}{1 + s^2 + 2s \cos(k_{\pm}x)}, \quad |s| < 1. \quad (2)$$

For $s = 0$, the potential $V_{\text{RP}\pm}(x, s)$ of amplitude U yields a sinusoidal shape; for $s > 0$, it provides an array of broad wells separated by narrow barriers; for $s < 0$, it provides deep narrow wells separated by broad flat barriers (see Fig. 1). $k_{\pm} = 2\pi/a_{\pm}$ are the wave-vector periodicities associated to the upper (−) and lower (+) substrates, and v_- , v_+ denote their sliding velocities respectively. γ

is a viscous-friction damping which takes into account various sources of dissipation in the substrates (phonons, electronic excitations, etc.), which are not explicitly included in the model. We select a relatively small dissipation constant $\gamma = 0.1$, producing an underdamped regime. As done in previous work [19, 20] to simulate an infinite system, periodic boundary conditions (PBC) are applied, implementing, e.g. via a continued fraction expansion technique [31], suitable rational approximations of the system periodicities a_+ , a_0 , and a_- , mimicking the desired incommensurability.

As found in earlier studies, the general behavior of this model depends crucially on the relative commensurability of the substrates and the chain (see Ref. [32] and references therein). To make a comparison with previous work in the sine-Gordon substrates, we consider here the corresponding ratios of length scales defined by $r = a_+/a_0 = N_0/N_+$ and $r' = a_-/a_+ = N_+/N_-$. r and r' are also expressed in terms of the number of lubricant particles N_0 and the numbers of periods N_{\mp} of the top/bottom potential oscillations in Eq. (1) within each simulation cell. For definiteness we take $r' > r^{-1}$ and $r' > 1$ so that the top substrate has the longest lattice spacing. We take $a_+ = 1$, $m = 1$, and the force $F_+ = 2\pi U/a_+$ as basic units for the model. In the following we express all physical quantities in terms of suitable combinations of a_+ , m , F_+ .

An adaptive fourth-order Runge-Kutta algorithm is used to integrate the equations of motion. We start off with the chain particles at equilibrium (the local energy minimum obtained by relaxing the immobile $-v_{\pm} = 0$ – system from a chain at rest with uniform separation a_0). Without loss of generality, we select a reference frame such that the bottom substrate is at rest ($v_+ = 0$), and make the upper substrate slide at constant velocity $v_- = V_{\text{ext}}$. After an initial transient, the system reaches a dynamical steady state characterized by regular or irregular fluctuations of the drift velocity of the chain particles around an average value, which we indicate by V_{CM} .

In the present work, we investigate the effects, on the tribological behavior of the sliding interface, of (i) the shape of the substrates potentials, represented by the RP parameter s , and (ii) the coverage Θ of the upper substrate to the array of kinks or antikinks. Since the mean distance between consecutive kink/antikinks is

$$d_{\text{kink}} = \frac{1}{\frac{1}{a_0} - \frac{1}{a_+}} = \frac{a_0}{1 - r^{-1}}, \quad (3)$$

this coverage

$$\Theta = \frac{a_-}{d_{\text{kink}}} = r' |r - 1| \quad (4)$$

can be tuned by modifying r' [24, 32].

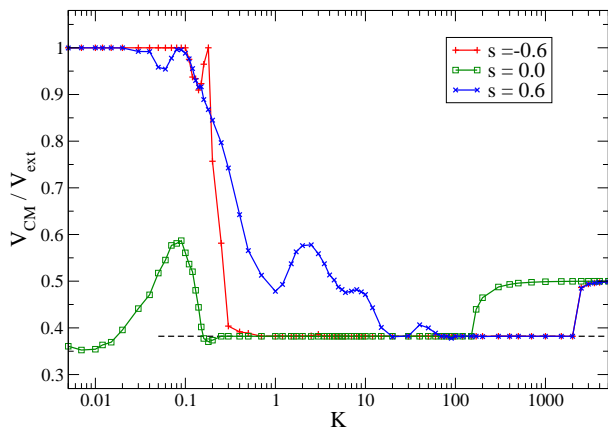


FIG. 2: (Color online) Ratio $V_{\text{CM}}/V_{\text{ext}}$ of the steady-state average chain center-mass velocity to the top speed, as a function of the chain stiffness K , for three values $s = -0.6, 0.0, 0.6$ of the potential shape parameter. The length ratios are taken as approximants to the golden mean $r = 377/233$, $r' = 233/144$; the simulation involves $N_0 = 377$ particles; the damping and top driving speed are $\gamma = 0.1$, $V_{\text{ext}} = 0.1$. The dashed line marks $w_{\text{plateau}} \simeq 0.382$.

III. RESULTS AND DISCUSSION

A. Kinks: lubricant forward motion

Figure 2 reports the time-averaged center-of-mass velocity V_{CM} of the chain (normalized to the top driving velocity V_{ext}) as a function of its stiffness K , for three values of the deformation parameter s . In this calculation, for the length ratios we take a rational approximant to the golden mean $r = \phi = (1 + \sqrt{5})/2 \simeq 1.62$. We adopt $\Theta = 1$, i.e. as many solitons as oscillation periods of the top substrate, and this, due to Eq. (4), implies $r' = 1/|r - 1|$. For $r \simeq \phi$, r' happens to approximate ϕ as well. According to Eq. (4), this choice for r' produces a coverage $\Theta = 1$, i.e. as many solitons as oscillation periods of the top substrate. The velocity of the sliding top substrate is set to a moderate $V_{\text{ext}} = 0.1$.

Within a broad range of stiffness values, the chain moves at the quantized velocity $V_{\text{CM}} = w_{\text{plateau}} V_{\text{ext}}$ [20], with

$$w_{\text{plateau}} = 1 - \frac{1}{r}, \quad (5)$$

approximately $w_{\text{plateau}} \simeq 0.382$ for the adopted value of r . For extremely soft harmonic interparticle couplings (small chain stiffness K) and for $s = -0.6$ or $s = 0.6$, the chain center of mass tends to move ahead at the full external velocity V_{ext} . In the opposite limit of a very stiff chain (large K), it moves at the symmetric speed $V_{\text{ext}}/2$. This is expected in a situation where the chain-corrugation interaction becomes marginal, and the dominating term in Eq. (1) is the dissipative one, which is minimum when $\dot{x}_i = (v_+ + v_-)/2 = V_{\text{ext}}/2$.

In the transitions between the plateau speed and the large- K and small- K regimes, the chain average velocity V_{CM} is generally a nontrivial function of the chain stiffness K . The effect of the shape of the corrugation potential is evident: for both positive and negative s , the plateau shrinks in size at the soft-chain side (small K), while it tends to expand in the stiff-chain side (large K). While the large- K expansion is the same for positive and negative s , the small- K shrinkage is far more dramatic for positive s , i.e. for broad shallow minima separated by narrow sharp maxima in the corrugation potential. Such a behavior can be qualitatively understood by considering that the plateau mechanism has been interpreted in terms of solitons, formed by the mismatch of the chain periodicity to that of the more commensurate substrate (here the bottom potential), being rigidly driven forward by the (top) advancing potential representing the other, more mismatched, sliding surface. As K is decreased, kinks become more and more localized objects: the plateau ends when the Peierls-Nabarro barrier [15] for a kink to move forward one lattice parameter approaches the single-particle activation energy to jump a corrugation potential barrier. When the two barriers coincide, no kink motion is granted any more, and the chain advances as a whole ($V_{\text{CM}} = V_{\text{ext}}$). For positive s values, the possibility for the particles to arrange relatively uniformly over the RP substrate at a small energy cost yields poorly localized kink superstructures in the chain, rapidly becoming equivalent to non-interacting particles, which are easily dragged forward, and drag the whole chain along. This rapidly destroys the quantized velocity plateau. In contrast, the deep narrow wells for negative values of the shape parameter s tend to compress the chain particles in sharper kink structures relatively more easily dragged along by the moving substrate, while leaving the other (non-soliton) particles still pinned in the other deep minima, and preserving the quantized motion down to softer K . The potential deformation is beneficial in the rigid-chain regime because, for given corrugation amplitude U , the maximum force (the slope at the inflection point, see Fig. 1) that the top potential can apply to the chain particles is larger for $s \neq 0$ than for the harmonic chain $s = 0$. The dragging force acting on the kinks is proportionally larger, allowing dragging to extend to stiffer chains which come with broader and fainter kinks.

To obtain a microscopic view of the quantized phenomena, we follow the motion of a particle of the chain and plot its velocity \dot{x}_i , aside with the CM velocity V_{CM} , as a function of time (left panels of Fig. 3). We compare the usual three values of the deformation parameter considered in simulations. We adopt relatively rigid stiffness $K = 100$ ($s = 0$) or 400 ($s = \pm 0.6$) selected to remain well inside the quantized plateau in all cases. The motion of a single particle is a periodic oscillation, representing the passage of a soliton across that specific particle. This period τ equals the distance d_{kink} between successive kinks divided by the speed V_{ext} at which

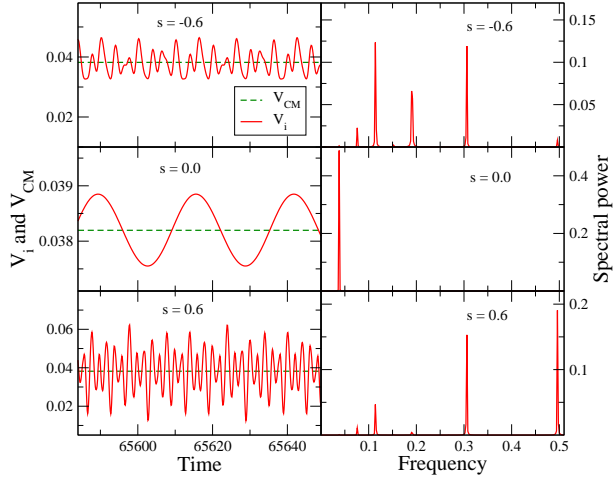


FIG. 3: (Color online) Left panels: time-evolution of the velocity of a particle V_i (solid) and the chain overall center of mass velocity V_{CM} (dashed), for three different shapes of the RP substrates potentials, and for stiffness $K = 100$ ($s = 0$) and $K = 400$ ($s = \pm 0.6$), representative of the quantized plateau. Right panels: the corresponding Fourier analysis of the velocity signal, representing the power spectral decomposition of the motion.

they are dragged forward by the advancing top substrate: $\tau = d_{\text{kink}} V_{\text{ext}}^{-1} = a_+ V_{\text{ext}}^{-1} (1 - 1/r)^{-1}$. Of course, this period is independent of the deformation parameter of the substrates. A Fourier analysis (right panels of Fig. 3) reveals that indeed the single-particle motion is periodic, with the same period $\tau = 1/\nu_0 \simeq 26.1$, where $\nu_0 \simeq 0.0382$ is the fundamental harmonic peak frequency in the Fourier spectrum of the present examples. However, the detailed motion induced by the deformed potential is clearly very different, characterized by a remarkably high harmonic contents, compared to the simple harmonic oscillation of the $s = 0$ case. The $s = \pm 0.6$ potential requires a complicated “dance” of the individual atoms to accommodate the passage of a soliton. Note also that the concerted oscillation of all particles in the chain makes its center of mass advance at an essentially constant speed (dashed line) $V_{CM}(t) \equiv w_{\text{plateau}} V_{\text{ext}}$ within numerical error.

To characterize in greater detail the effect of the potential shape on the quantized motion, we investigate the upper and lower boundary of the quantized plateau, K_{Max} and K_{Min} respectively. These boundaries are obtained by a sequence of linked calculations carried out with increasing (for K_{Max}) or decreasing (for K_{Min}) K in small steps, until the quantized plateau is abandoned. For example, the sequence of calculations of Fig. 2 shows that $K_{\text{Max}} \simeq 2000$ for $s = \pm 0.6$. Figure 4 reports the dependency of K_{Min} and K_{Max} on the potential shape parameter s . K_{Max} is a symmetric function of the shape parameter s . In contrast, the K_{Min} curve is quite asymmetric. As already remarked above, at the soft-chain side positive s is consistently detrimental to the plateau

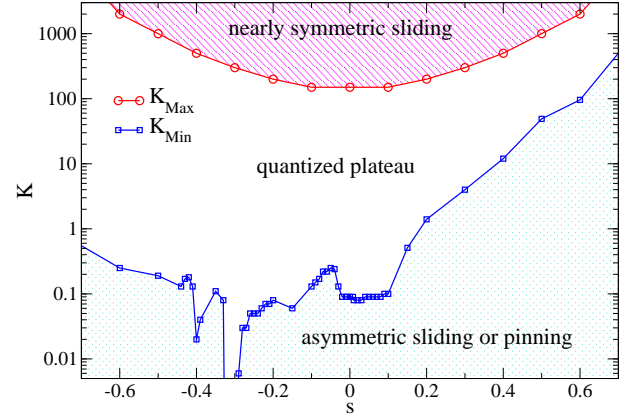


FIG. 4: (Color online) The boundaries K_{Min} and K_{Max} of the quantized velocity plateau as a function of the chain stiffness K , for varied potential shape parameter s . The model conditions are the same as in Fig. 2.

state, leading to a rapid (approximately exponential) increase of K_{Min} with s . In contrast, the negative- s region has a range $-0.4 < s < -0.2$ where the potential shape deformation is beneficial to the quantized plateau even for soft chains. A further decrease of s to more negative values produces an increase of K_{Min} , but a slow one, such that the relative width $K_{\text{Max}}/K_{\text{Min}}$ of the plateau actually increases as s decreases. The K_{Min} and K_{Max} curves delimit the quantized velocity plateau region in the space of parameters s and K . Above this region, we find a stiff-chain region where the dynamics is dominated by the dissipative term in Eq. (1), and V_{CM} approaches rapidly $V_{\text{ext}}/2$, with the two sliders acting symmetrically on the chain. The soft-chain region below the K_{Min} exhibits occasional pinning to either the top or the bottom slider, or unpinning nonquantized nonperiodic orbits.

The “dynamical phase diagram” of Fig. 4 is relevant for the specific adopted value of dissipation γ and of speed V_{ext} . A modification of these two parameters would indeed modify the shape of the diagram, while preserving its overall features.

B. Antikinks: lubricant backward motion

When $r < 1$, i.e. when lubricant particles are fewer than the minima in the static substrate ($N_0 < N_+$), Eq. (5) predicts that the lubricant velocity turns negative, i.e. opposite to V_{ext} . This remarkable leftward motion, produced by rightward moving antikinks is indeed observed even for the deformed RP potential, as shown in the example of Fig. 5. The resulting “backward” plateaus are not so wide as in the case of kink-assisted forward lubricant motion. This qualitative finding, quite likely to carry forward to experiment is due to the dissipation into the substrate represented by the last term in Eq. (1) which tend to favor a positive “sym-

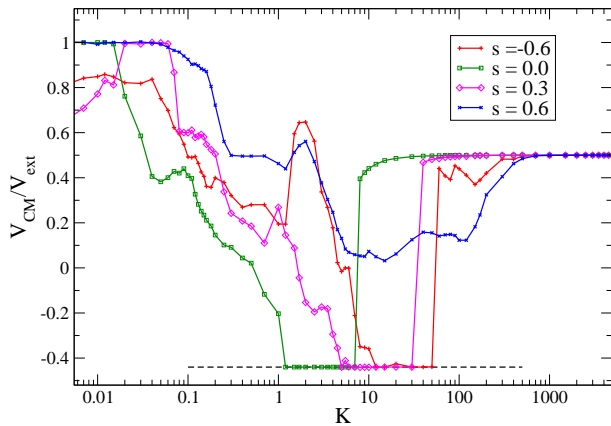


FIG. 5: (Color online) Antikink geometry, for $r = 25/36 < 1$: the average center-mass velocity $V_{\text{CM}}/V_{\text{ext}}$ of the lubricant chain as a function of its stiffness K . Note the negative-velocity plateau, representing a leftward lubricant motion. The other parameters are $V_{\text{ext}} = 0.1$, $r' = 36/11$, and the model is simulated taking $N_+ = 144$, $N_0 = 100$ and $N_- = 44$, for deformations $s = -0.6, 0.0, 0.3$, and 0.6 . The dashed line marks $w_{\text{plateau}} = -0.44$.

metric” speed $V_{\text{CM}} \simeq V_{\text{ext}}/2$, thus actively disturbing the $V_{\text{CM}} < 0$ quantized motion. Like in the $r = \phi$ case, the plateau width and K range depends quite sensitively on the deformation parameter s . In particular positive s is also especially effective in disrupting the plateau, and indeed for very strong deformation $s = 0.6$ the backward plateau disappears altogether, the top driving substrate being unable to grab and drag the antikink pattern in the confined chain.

C. The effect of coverage

The choices of r' adopted in the calculations of both Figs. 2 and 5 produce coverage $\Theta = 1$, i.e. as many solitons (or antisolitons) as periodic oscillations of the top slider. As was pointed out [33, 34], such perfect matching is the most favorable for kinks (or antikinks) dragging, thus for the quantized sliding phenomenon. To investigate how releasing the $\Theta = 1$ matching condition affects the lubricant dynamics, we compare several calculations with the same r but with different values of the coverage obtained by changing r' , i.e. the top substrate lattice spacing a_- .

To investigate the coverage dependency, we consider fixed $r = 377/233$ and the following values of r' : 233/180, 233/144 and 233/72 corresponding to kink coverage $\Theta = 0.8$, $\Theta = 1$ and $\Theta = 2$ respectively. The results of these calculations are displayed in Fig. 6 for three values of the shape parameter. It can be seen that, independently on the value of the deformation parameter s , the kink coverage largely affects the plateau by reducing its width as soon as the full matching (unit coverage) is lost. In gen-

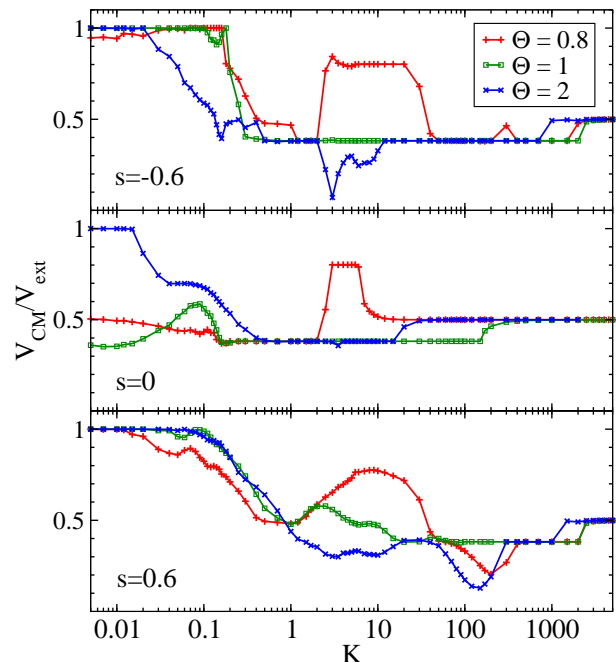


FIG. 6: (Color online) Normalized center-mass velocity, $V_{\text{CM}}/V_{\text{ext}}$ as a function of the stiffness K , for three values of the deformation parameter. The simulations are carried out for $N_0 = 377$ particles in $N_+ = 233$ bottom wells with $N_- = 180, 144$, and 72 , producing coverage $\Theta = 0.8, 1$, and 2 respectively. Note the shrinkage of the plateau for $\Theta \neq 1$, quite substantially so for $\Theta = 0.8$.

eral, for the less commensurate the kink coverage $\Theta = 0.8$ the plateau is disrupted quite substantially. Not surprising, for the commensurate $\Theta = 2$ this reduction is less significant. Still, for $\Theta = 2$ only one kink out of two finds a top corrugation which drags it along: accordingly, a plateau shrinkage is observed nonetheless.

We have carried out similar simulations for other commensurability ratios, e.g. the value $r = 25/36$ considered in Sect. IIIB. The conclusion is that the quantized plateau always shrinks, often to the point of disappearing, whenever $\Theta \neq 1$.

IV. CONCLUSIONS

In this work, we study the effect of the potential shape on the dynamics of a sliding 2-substrate FK-type model. Even though this deformation goes a modest step away from the idealized world of models in the direction of real friction, it provides some useful trends and general understanding. In particular, we establish that in the rigid-lubricant limit (large K) the worst possible pinning scheme for the solitons is that granted by a sinusoidal corrugation. Any kind of deformation is beneficial to the quantized state. This is quite remarkable also in view of the fact that this rigid-lubricant regime is relevant

whenever the lubricant-lubricant in-plane forces dominate over the substrate corrugation, e.g. for noble-gases layers driven over graphite or even over several metallic surfaces [35–37]. On the opposite, soft-lubricant limit instead a sinusoidal surface corrugation tends to be optimal, although a pattern based on narrow (but not too narrow wells may occasionally provide even more favorable conditions for the quantized lubricant state.

The grabbing of kinks by the more rarefied top slider is best seen when the kink lattice is fully commensurate to the top. Whenever this is not the case (kink coverage deviating from unity) the quantization phenomenon becomes less prominent. However, this observation is to be integrated by a further point. As illustrated in the upper and central panels of Fig. 6, secondary plateaus can arise V_{CM} values different from those predicted by the quantized formula (5). For example, in the $\Theta = 0.8$ simulations producing the secondary plateau characterized by $V_{CM}/V_{ext} \simeq 0.802$, individual particles do carry out regular periodic trajectories, like in the standard quantized state. These secondary plateaus, observed also for the purely sinusoidal corrugation [21, 38], are likely to

be due to resonances very much akin to Shapiro steps [15, 39–41], excited by the simultaneous action of the periodically oscillating force produced by the sliding substrate and the forward-dragging force produced by the dissipative term in Eq. (1). Further investigation of such secondary plateaus can lead to better insight in their nature, and possibly find realistic configurations where they could arise, e.g. in colloidal sliding [42–45].

Acknowledgement

RLW is grateful to the Abdus Salam International Centre for Theoretical Physics (ICTP) where a part of this work was carried out during her visit under the associate federation scheme. The authors thank E. Tosatti and G. E. Santoro for collaboration, discussion, and continuing support. This work was partly sponsored by Sinergia CRSII2_36287/1, and by advances of ERC Advanced Grant No. 320796-MODPHYSFRICT.

-
- [1] F. P. Bowden and D. Tabor, *The Friction and Lubrication of Solids* (Oxford Univ. Press, New York, 1950).
 - [2] B. N. J. Persson, *Sliding Friction, Physical Properties and Applications* (Springer, Berlin, 2000).
 - [3] S. M. Rubinstein, G. Cohen, and J. Fineberg, *Nature* (London) **430**, 1005 (2004).
 - [4] S. M. Rubinstein, G. Cohen, and J. Fineberg, *Phys. Rev. Lett.* **96**, 256103 (2006).
 - [5] M. O. Robbins and M. H. Müser, in *Modern Tribology Handbook*, edited by B. Bhushan (CRC Press, Boca Raton, Florida, 2001), p. 717.
 - [6] O. M. Braun and A. G. Naumovets, *Surf. Sci. Rep.* **60**, 79 (2006).
 - [7] O. M. Braun, N. Manini, and E. Tosatti, *Phys. Rev. B* **78**, 195402 (2008).
 - [8] F. Bonelli, N. Manini, E. Cadelano, and L. Colombo, *Eur. Phys. J. B* **70**, 449 (2009).
 - [9] C. Negri, N. Manini, A. Vanossi, G. E. Santoro, and E. Tosatti, *Phys. Rev. B* **81**, 045417 (2010).
 - [10] O. M. Braun, N. Manini, and E. Tosatti, *Phys. Rev. Lett.* **110**, 085503 (2013).
 - [11] A. Vanossi, N. Manini, M. Urbakh, S. Zapperi, and E. Tosatti, *Rev. Mod. Phys.* **85**, 529 (2013).
 - [12] R. W. Carpick and M. Salmeron, *Chem. Rev.* **97**, 1163 (1997).
 - [13] M. Dienwiebel, G. S. Verhoeven, N. Pradeep, J. W. M. Frenken, J. A. Heimberg, and H. W. Zandbergen, *Phys. Rev. Lett.* **92**, 126101 (2004).
 - [14] J. Krim, *Adv. Phys.* **61**, 155 (2012).
 - [15] L. M. Floría and J. J. Mazo, *Adv. Phys.* **45**, 505 (1996).
 - [16] O. M. Braun and Yu. S. Kivshar, *The Frenkel-Kontorova Model: Concepts, Methods, and Applications* (Springer-Verlag, Berlin, 2004).
 - [17] M. Peyrard and S. Aubry, *J. Phys. C: Solid State Phys.* **16**, 1593 (1983).
 - [18] *Superlubricity*, ed. by A. Erdemir, J.-M. Martin (Elsevier, Amsterdam, 2007).
 - [19] O. M. Braun, A. Vanossi, and E. Tosatti, *Phys. Rev. Lett.* **95**, 026102 (2005).
 - [20] A. Vanossi, N. Manini, G. Divitini, G. E. Santoro, and E. Tosatti, *Phys. Rev. Lett.* **97**, 056101 (2006).
 - [21] G. E. Santoro, A. Vanossi, N. Manini, G. Divitini, and E. Tosatti, *Surf. Sci.* **600**, 2726 (2006).
 - [22] M. Cesaratto, N. Manini, A. Vanossi, E. Tosatti, and G. E. Santoro, *Surf. Sci.* **601**, 3682 (2007).
 - [23] A. Vanossi, G. E. Santoro, N. Manini, M. Cesaratto, and E. Tosatti, *Surf. Sci.* **601**, 3670 (2007).
 - [24] N. Manini, M. Cesaratto, G. E. Santoro, E. Tosatti, and A. Vanossi, *J. Phys.: Condens. Matter* **19**, 305016 (2007).
 - [25] A. Vanossi, G. E. Santoro, N. Manini, E. Tosatti, and O. M. Braun, *Tribol. Int.* **41**, 920 (2008).
 - [26] M. Remoissenet and M. Peyrard, *J. Phys. C* **14**, L481 (1981).
 - [27] M. Peyrard and M. Remoissenet, *Phys. Rev. B* **26**, 2886 (1982).
 - [28] G. Djuidje Kenmoe, A. Kenfack Jiotso, and T. C. Kofan, *Physica D: Nonlinear Phenom.* **191**, 31 (2004).
 - [29] B. Hu and J. Tekić, *Phys. Rev. E* **72**, 056602 (2005).
 - [30] R. L. Woulaché, D. Yemélé, and T. C. Kofané, *Phys. Rev. E* **72**, 031604 (2005).
 - [31] A. Ya. Khinchin, *Continued Fractions* (Dover, New York, 1997).
 - [32] N. Manini, A. Vanossi, G. E. Santoro, and E. Tosatti, *Phys. Rev. E* **76**, 046603 (2007).
 - [33] A. Vanossi and O. M. Braun, *J. Phys.: Condens. Matter* **19**, 305017 (2007).
 - [34] I. E. Castelli, N. Manini, R. Capozza, A. Vanossi, G. E. Santoro, and E. Tosatti, *J. Phys.: Condens. Matter* **20**, 354005 (2008).
 - [35] L. W. Bruch, R. D. Diehl, and J. A. Venables, *Rev. Mod. Phys.*

- Phys. **79**, 1381 (2007).
- [36] S. R. Sharma, S. F. O'Shea, and W. J. Meath, Phys. Rev. B **40**, 6356 (1989).
 - [37] J. Lv, M. Bai, W. Cui, and X. Li, Nanoscale Res. Lett. **6**, 200 (2011).
 - [38] N. Manini, G. E. Santoro, E. Tosatti, and A. Vanossi, J. Phys.: Condens. Matter **20**, 224020 (2008).
 - [39] J. Tekić and B. Hu, Appl. Phys. Lett. **95**, 073502 (2009).
 - [40] J. Tekić and Z. Ivić, Phys. Rev. E **83**, 056604 (2011).
 - [41] P. Mali, J. Tekić, Z. Ivić, and M. Pantić, Phys. Rev. E **86**, 046209 (2012).
 - [42] T. Bohlein, J. Mikhael, and C. Bechinger, Nature Mater. **11**, 126 (2012).
 - [43] T. Bohlein and C. Bechinger, Phys. Rev. Lett. **109**, 058301 (2012).
 - [44] A. Vanossi and E. Tosatti, Nature Mater. **11**, 97 (2012).
 - [45] A. Vanossi, N. Manini, and E. Tosatti, P. Natl. Acad. Sci. USA **109**, 16429 (2012).